NUCL SCI TECH (2016) 27:135
DOI 10.1007/s41365-016-0136-0

Readout electronics of a prototype spectrometer for measuring low-energy ions in solar wind plasma

Di Yang[1,2] · Zhe Cao[1,2] · Xi Qin[2] · Xin-Jun Hao[3,4] · Shu-Bin Liu[1,2] · Chang-Qing Feng[1,2] · Qi An[1,2]

Received: 4 April 2016 / Revised: 24 June 2016 / Accepted: 5 July 2016 / Published online: 12 October 2016

Abstract Readout electronics is developed for a prototype spectrometer for in situ measurement of low-energy ions of 30 eV/e–20 keV/e in the solar wind plasma. A low-noise preamplifier/discriminator (A111F) is employed for each channel to process the signal from micro-channel plate (MCP) detectors. A high-voltage (HV) supply solution based on a HV module and a HV optocoupler is adopted to generate a fast sweeping HV and a fixed HV. Due to limitation of telemetry bandwidth in space communication, an algorithm is implemented in an FPGA (field programmable gate array) to compress the raw data. Test results show that the electronics achieves a 1 MHz event rate and a large input dynamic range of 95 pC. A slew rate of 0.8 V/μs and an integral nonlinearity of 0.7-LSB for the sweeping HV, and a precision of less than 0.8 % for the fixed HV are obtained. A vacuum beam test shows an energy resolution of 12 ± 0.7 % full width at half maximum (FWHM) is achieved, and noise counts are less than 10/sec, indicating that the performance meets the physical requirement.

Keywords Solar wind plasma · Energy spectrometer · Readout electronics · A111F · Data compression

1 Introduction

Solar wind, a plasma stream from the upper atmosphere of the Sun, mainly consists of protons, electrons, helium ion, and other ions in a whole spectrum of ionization states [1]. The energy spectra of the ions is indispensable for observing solar wind activity, and important for exploring the source of the particles accelerated to produce the shock associated and storm ions and so on [2, 3].

A low-energy ion prototype spectrometer is being developed to measure solar wind ions in the interplanetary space. It will cover the energy-per-charge range of 30 eV/e ∼ 20 keV/e in an energy resolution ($\Delta E/E$) of better than 15 % (FWHM). As shown schematically in Fig. 1, it contains three structural elements: an entrance unit, a particle detection unit, and its readout electronics.

The entrance unit is implemented by a symmetrical electrostatic analyzer (ESA) with a top hat, which is used to select incident ions at 32 energy steps controlled by the sweeping HV between its inner hemisphere and outer hemisphere. The detection unit, with a gain factor of about 10^6, mainly comprises of two MCP multipliers in a chevron pair configuration and 12 position encoding discrete anodes which present the azimuth information, leading to 12 readout channels of the electronics.

Low-energy ions contribute most of the particle flux of solar wind, thus a large number of event signals are

This work was supported by the National Key Scientific Instrument and Equipment Development Projects of the National Natural Science Foundation of China (No. 41327802) and the Fundamental Research Funds for the Central Universities (WK2030040066).

✉ Chang-Qing Feng
fengcq@ustc.edu.cn

[1] State Key Laboratory of Particle Detection and Electronics (IHEP-USTC), Hefei 230026, China

[2] Department of Modern Physics, University of Science and Technology of China, Hefei 230026, China

[3] Division of Space Physics, University of Science and Technology of China, Hefei 230026, China

[4] CAS Key Laboratory of Geospace Environment, Hefei 230026, China

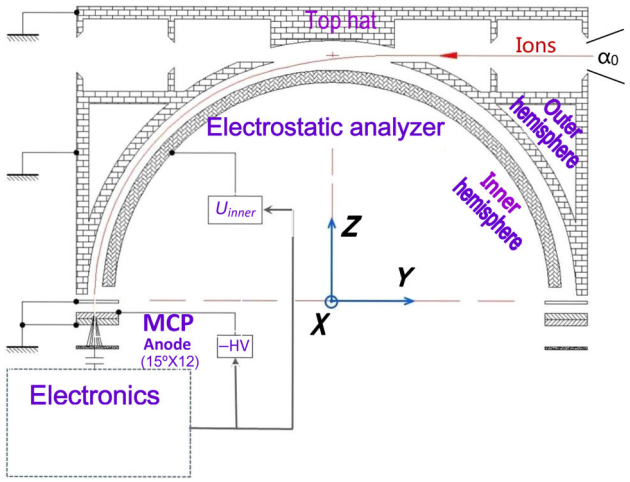

Fig. 1 Structural diagram of prototype spectrometer

generated by the MCP detector, imposing a challenge on the readout electronics [3, 4]. Meanwhile, to get the actual events, background noise must be rejected efficiently. A fast sweeping HV ranging from −2300 to −3.5 V and a fixed HV at −2500 to −2300 V are required to apply to the ESA and MCP, respectively. Event signals of each channel at every energy step are counted by the electronics, which brings a data rate close to 15 kbps after count accumulation in one spin period of the spacecraft. Nevertheless, the transmission width allocated to the spectrometer is only 3.2 kbps, as the telemetry bandwidth between satellite and ground is confined in space mission. So an efficient algorithm is needed to compress the raw data with low distortion. Besides, the reliability of electronics has to be considered because of the space radiation environment.

In this paper, we report the design of readout electronics to fulfill the requirements of spectrometer and the performance test.

2 Electronics design

According to principle of the spectrometer, the main function of the readout electronics is to count MCP signals of each channel at different energy steps controlled by a HV supply circuit. In addition to high-event rate, a low-noise level of the readout electronics is required to satisfy the demand of the energy resolution that is also devoted to by the ESA and MCPs. And the low-noise level is critical, too, for its key role in threshold setting of discrimination.

Some space programs used the front-end electronics to read detector signals, such as the Double Star mission [5], Spektr-R [6], CAPS [7], and CLUSTER [8]. In the Double Star and Spektr-R, the detector signals are amplified by A225 with a low-noise charge sensitive amplifier and a fast shaper with a high-count rate, and then discriminated by a comparator that outputs a digital pulse to a counter. Obviously, this readout scheme is not suitable for this application of low power consumption and tightly restricted space. Efforts have been made in improving the integration of readout electronics for space plasma instruments, such as developing a multi-channel, mixed-signal integrated circuit (IC) AIDA [9, 10]. However, the radiation effects of semiconductor devices, especially the single events effect (SEE) and the total ionizing dose (TID), have to be taken into account [11]. Thus, few of the multi-channel application special integration circuits (ASICs) are practical in the harsh space environment. In CAPS, an A111F was used as a charge sensitive preamplifier/discriminator, while in CLUSTER an A121 was used. Although they are single channel circuits, their reliability and counting rate satisfy the physical demand. Considering the power limit, the noise level and the telemetry rate constraint, a readout scheme based on A111F chips and RS422 interface, together with a HV supply circuit, is adopted for the Low-Energy Ion Spectrometer.

As shown in Fig. 2, the top-level diagram of the readout electronics is mainly composed of the preamplifier & discriminator circuits, HV supply module, self-test circuitry, and control and data processing unit.

2.1 Preamplifier and discriminator circuits

The preamplifier and discriminator are implemented by the A111F hybrid chip. Due to the number of discrete anodes, 12 A111F chips are employed. Besides its high counting rate (∼2.5 MHz) and low noise (0.44 fC for nominal threshold) performance, the A111F features a high sensitivity (8 fC), a 25 ns rise-time and a small size (occupying less space on the printed circuit board) [12]. And the discrimination threshold in the A111F is adjustable to filter non-interesting events. Although anode strips are connected to ground level via large resistors, a 1-nF high-voltage capacitor and a pair of clamping diodes are utilized at the input pin of A111F, to avoid possible high-voltage discharge.

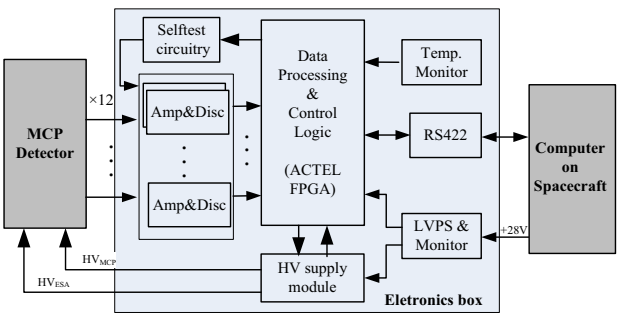

Fig. 2 Top-level diagram of the readout electronics

2.2 HV supply module

The HV supply module is designed to generate a sweeping HV and a fixed HV. Prior to event signals produced by the MCPs, a sweeping HV of −2300 to −3.5 V is applied to the ESA, and a fixed HV at −2500 to 2300 V for biasing the MCPs. It includes a digital-to-analog converter (DAC), two amplifiers, a high-voltage optocoupler, an HV module, an analog-to-digital converter (ADC) and some voltage-proof resistors, as shown in Fig. 3 [13]. It generates a −3000 V output, which is divided by a resistor divider to get the fixed HV, meanwhile, is led to a fast HV optocoupler to generate the sweeping HV controlled by a DAC.

2.3 Self-test circuitry

To check operating status of signal chains of the readout electronics in a complex and harsh space environment, a built-in self-test circuitry is utilized (Fig. 4). The DAC is controlled by an FPGA to output an adequate analog voltage. A narrow signal enables the analog switch to turn on, producing a test pulse to trigger A111Fs by capacitive coupling. Apart from checking the operating status, the data compress algorithm in FPGA can also be verified by accommodating the frequency of the test pulse.

2.4 Control and data processing unit

The control and data processing unit is implemented in FPGA (ACTEL Corp.). Its block diagram is shown in Fig. 5. In order to make the instrument into operative mode, related commands, sent by an upper computer and arriving at the subcell manage block after UART receiving and command parsing, are used to control or configure DACs, ADCs and other components orderly. When entering into counting mode, 12 counters (24-bit) record the event signals which are from A111Fs at the period of corresponding energy step for each channel. Then the 12 counting values at each energy step are accumulated cycle by cycle, respectively. After 64 cycles per spin, the last

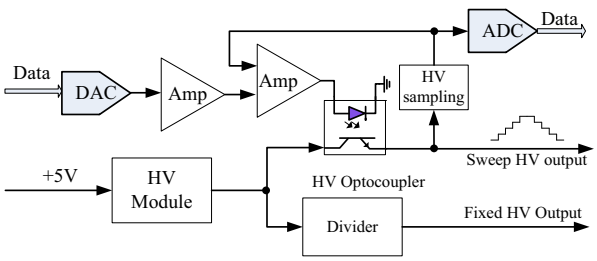

Fig. 3 Scheme of HV supply module

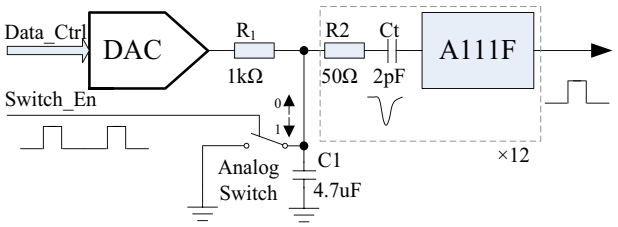

Fig. 4 Simplified diagram of self-test circuitry

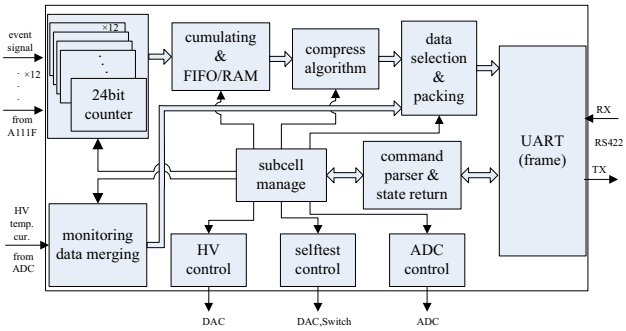

Fig. 5 Block diagram of the control and data processing unit

accumulated values of 24-bit raw data are compressed into 8-bit data by a log compression algorithm [14]. The decompression is given by Eq. (1), and the maximum loss rate is less than 8 %. There is about 15 K bit/s transmission rate without data compression, which surpasses considerably the 3.2 K telemetry width. While counters are counting, the status of HV supply and low power operating current, and the ambient temperature, are collected. Under different working modes, the compressed event data, or the monitoring data, or both, is sent to the upper computer after data packing and framing

$$\begin{aligned} M &= N \quad \text{when } N < 32 \\ N_1 &= (M[3:0] + 16) \times 2^{M[7:4]} \quad \text{when } N > 32 \end{aligned} \tag{1}$$

where, N is a raw 24 bit count datum, M is a 8 bit output code after compression, and N_1 is a datum after decompression.

Considering the dead time τ ($<0.6 \times 10^{-6}$s) of the signal chain, the true counting rate is then:

$$R = N_1/(1 - N_1\tau) \tag{2}$$

3 Results

The prototype detector and readout electronics are shown in Fig. 6a, b, respectively. An electronics test system and an ion beam test system are established for the performance test (Fig. 6c), and the electronics test is shown schematically in Fig. 6d.

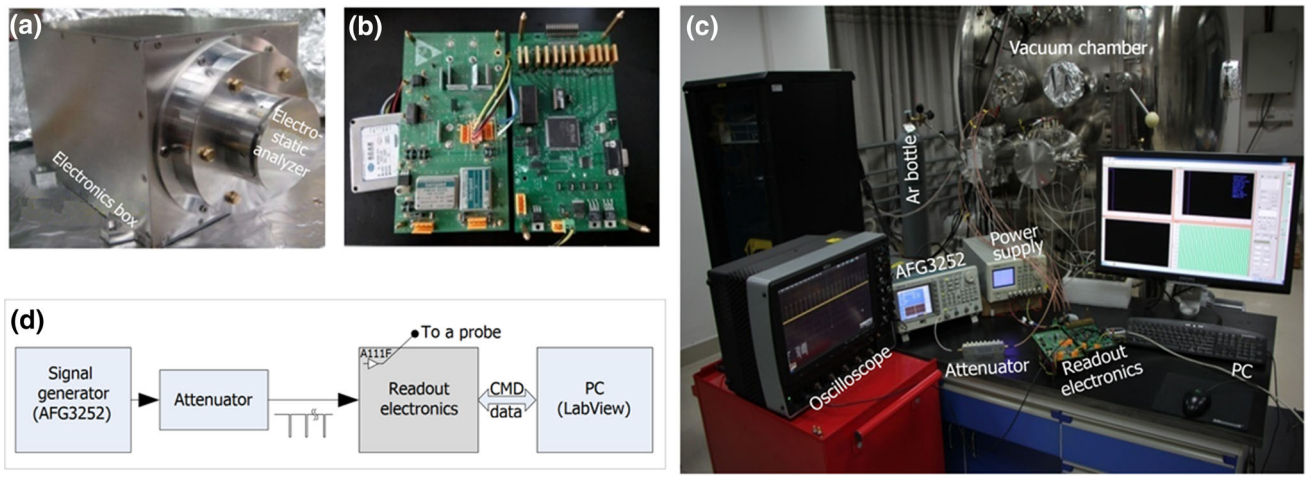

Fig. 6 Prototype detector (**a**), the readout electronics (**b**), the test systems (**c**), and schematics of the electronics test setup (**d**)

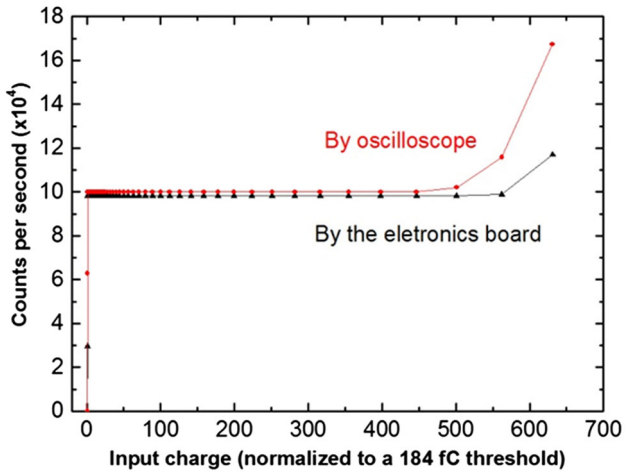

Fig. 7 Input dynamic range

3.1 Electronics test

As shown in Fig. 6d, a signal generator (TEK AFG3252), together with a passive attenuator, outputs an appropriate negative pulse to preamplifiers in the electronics. The counting data are transferred to a remote PC for further analysis and display executed by a LabView program. An oscilloscope is used to measure the output signal for comparison. Against the background noise and crosstalk, an 184 fC threshold is configured for A111Fs. Under the condition of a 100 kHz narrow test signal, the input dynamic range expressed as the normalized threshold, is achieved by regulating the amplitude of input signal and the attenuation ratio. Figure 7 shows the counting rate verse the input charge, measured by both the readout electronics and the oscilloscope. There is a stable and flat count rates, about 98.3 kHz by the electronics and 100 kHz

Table 1 Detection efficiency of readout electronics

Event rate[a] (Hz)	By oscilloscope (Hz)	By Eqs. (1, 2) (counts/sec)	Detection efficiency (%)
1024,000	1023,980	973,677.7	95.09
512,000	511,992	486,838.9	95.09
256,000	255,996	243,419.4	95.09
128,000	127,998	121,709.7	95.09
65,536	65,535	63,195.4	96.43
32,768	32,768	31,597.7	96.43
16,384	16,384	15,798.9	96.43
4096	4096	3949.7	96.43
1024	1024	994.3	97.10
512	512	497.1	97.10
64	64	62.9	98.21

[a] Generated by built-in circuit

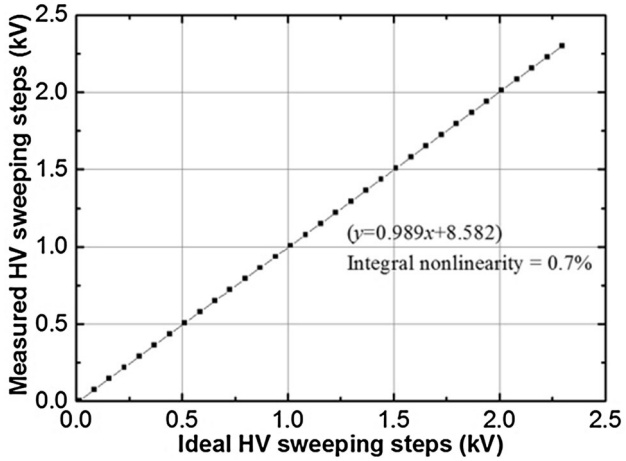

Fig. 8 Correlation between tested step values and ideal step values

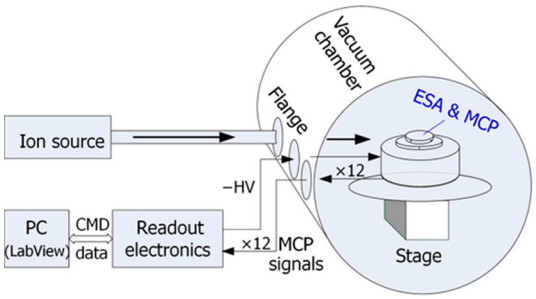

Fig. 9 Diagram of the beam test system. The sensor lies on a stage in the vacuum chamber, while the readout electronics is outside

by the oscilloscope, in a wide input range from a 184 fC threshold to 95 pC (over 500 times of the threshold). For both ways of measurement, the counting rate drops sharply below the threshold of input, while it increases noticeably at input charges beyond 95 pC, which will be explained in Section IV.

With a suitable width-fixed test pulse generated by the built-in test circuit to trigger A111Fs, detection efficiency of the readout electronics at different event rates can be measured by adjusting the frequency of test signal which is accomplished by a self-test control unit in the FPGA via sending different control commands. The detection efficiencies at expected event rates are listed in Table 1, which verifies the log compression algorithm.

A linear sweeping test and a fixed voltage deviation test are conducted for the HV supply module, with a relative precision of <0.8 % for fixed HV, a 0.7 % integral nonlinearity (Fig. 8), and a fast enough slew rate (0.8 V/μs) for the sweeping HV. More details can be found in Ref. [13].

3.2 Beam tests

A beam test system under ground-based vacuum facility is constructed to simulate the vacuum environment in space, as shown in Fig. 9. The ion source injects a 2.5 keV Ar^+ beam into the vacuum chamber, which covers the whole effective area of the sensor aperture. With the MCPs biased at −2500 V, the ESA is controlled to sweep in −150 to − 400 V to select the incident Ar^+ beams.

Figure 10a shows the energy response represented by the counting rates of relevant channels. The energy resolution ($\Delta E/E$) is 12 ± 0.7 % (FWHM) for Channel 8 by a Gaussian fitting (dashed curve). Figure 10b shows the baseline noise measurement with the ESA sweeping from −100 to −800 V for Ch7 to Ch9. The noise counts is less than 10/sec.

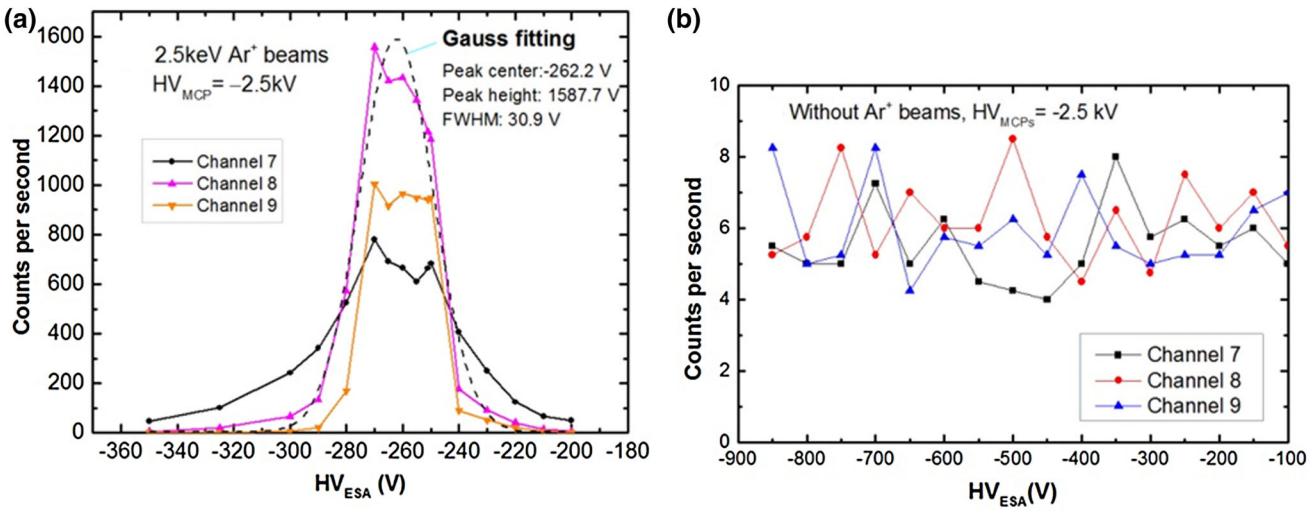

Fig. 10 Energy response (**a**) and noise level (**b**) from Ch7 to Ch9

4 Discussion

4.1 Input dynamic range and double pulsing effect

Test results confirm that the readout electronics reaches an input dynamic range from 184 fC to 95 pC, as the counting rate is flat and accords with the compression algorithm which can be verified by a built-in circuit generating test pulses up to 1 MHz. The increase in counting rate with input charges beyond 95 pC is due to the double pulsing, which was also observed by Iliev Metodi et al. [15].The double pulsing is yielded by the shape variation which creates the possibility that under the large input signals, the discriminator threshold may be crossed more than once during the duration of the pulse.

4.2 Energy resolution

In the Ar^+ beam test, sizeable flux of Ar^+ beams is injected into Ch8 and the counting rate of each channel is compared. The noise counting under different sweeping HV can manifest that the spectrometer is of low noise, since the count rate fits comfortably with the dark counts of MCP [16]. Due to the optimized ion optics design of the ESA and a low-noise level, an energy resolution $\Delta E/E$ of 12 ± 0.7 % (FWHM) is achieved, which is better than the design specification of 15 %.

4.3 Consideration for radiation mitigation

Because of the radiation environment in space, hazards can be imposed to the readout electronics. For example, TID can affect input bias current, offset voltage, transistor parameters, timing margins and so on for microcircuits, while SEEs can upset the logic state, cause malfunctions or even latch-up [17]. Apart from shielding, components with high TID tolerance have a higher priority during this electronics design. For example, A111F and LM6142 (operational amplifier) have a TID resistance over 100kRad (Si). There are also other measures to mitigate SEEs, such as adding current-limiting resistors to the input and power-supply pins of a component to reduce latch-up currents, using triple module redundancy (TMR) and parity check techniques for FPGA logic [18]. Some anti-fuse and Flash FPGA are much more suitable for aerospace applications because their logic elements are immune to SEE. For example, Actel ProASIC PLUS series Flash-based FPGAs are tolerant to single event upset (SEU), and their linear energy transfer (LET) threshold for single event latch-up (SEL) is over 104 (MeV-cm2/mg) [19]. However, in this prototype design, considering the cost and practical requirements, some commercial components including an FPGA are used instead of high-reliable ones. The detailed design of radiation mitigation and verification test will be a focus in the future version.

5 Conclusion

A readout electronics has been developed for a prototype of low-energy spectrometer to measure the solar wind plasma in the energy range from 30 eV/e to 20 keV/e. An electronics test and a primary beam test have been completed and show that the readout electronics works steadily. A fine energy resolution, a high-count rate with low distortion and a large input range can demonstrate that the electronics satisfies the physical requirements of the energy spectrometer. Right now, the electronics has been successfully assembled with the prototype detector for further vacuum experiment.

Acknowledgments The authors are grateful for the support of collaboration team from CAS Key Laboratory of Geospace Environment (USTC).

References

1. A.J. Hundhausen, *Coronal expansion and solar wind* (Springer Science & Business Media, Berlin, 2012), pp. 109–111
2. S.I. Akasofu, A historical review of the geomagnetic storm-producing plasma flows from the Sun. Space Sci. Rev. **164**, 85–132 (2011). doi:10.1007/s11214-011-9856-y
3. R.P. Lin, K.A. Anderson, S. Ashford et al., A three-dimensional plasma and energetic particle investigation for the wind spacecraft. Space Sci. Rev. **71**, 125–153 (1995). doi:10.1007/BF00751328
4. A.B. Galvin, L.M. Kistler, M.A. Popecki et al., The plasma and suprathermal ion composition (PLASTIC) investigation on the STEREO observatories. Space Sci. Rev. **136**, 437–486 (2008). doi:10.1007/s11214-007-9296-x
5. S. McKenna-Lawlor, J. Balaz, I. Strharsky et al., The energetic NeUtral atom detector unit (NUADU) for China's double star mission and its calibration. Nucl Instrum Methods A **530**, 311–322 (2004). doi:10.1016/j.nima.2004.04.244
6. J. Balá, I. Strharsky, Programmable energetic particle spectrometer MEP 2 for space project spectrum—RADIOASTRON. Report number, UEF-01-11. doi: 10.13140/RG.2.1.2207.6000 (2015)
7. D.T. Young, B.L. Barraclough, J.J. Berthelier et al., Cassini plasma spectrometer investigation. Space Sci. Rev. (2004). doi:10.1007/s11214-004-1406-4
8. H. Reme, C. Aoustin, J.M. Bosqued et al., First multispacecraft ion measurements in and near the earth's magnetosphere with the identical cluster ion spectrometry(CIS) experiment. Ann. Geophys. **19**, 1303–1354 (2001). doi:10.5194/angeo-19-1303-2001
9. A. Rhouni, J.D. Techer, G. Sou et al., A high dynamic range and low power 16-channel CMOS circuit for particle detection in space plasmas. IEEE IMTC P (2012). doi:10.1109/I2MTC.2012.6229513
10. V.B. Cajipe, J.H. Clemmons, M. Clajus et al., in *Multi-channel charge amplifier-discriminator-counter IC for the space sciences.*

IEEE nuclear science symposium conference record, vol. 3, 1605–1608 (2006). doi: 10.1109/NSSMIC.2006.354204
11. S.S. Gao, C.Q. Feng, D. Jiang et al., Radiation tolerance studies on the VA32 ASIC for DAMPE BGO calorimeter. Nucl. Sci. Tech. **25**, 010402 (2014). doi:10.13538/j.1001-8042/nst.25.010402
12. A111F hybrid charge sensitive preamplifier, discriminator, and pulse shaper. Amptek Inc., USA. http://www.amptek.com/a111.html
13. D. Yang, Z. Cao, X. Qin, et al., Design of the high voltage supply module of a prototype energy spectrometer for solar wind plasma measurement. The 34th international cosmic ray conference (Hague, Netherlands), p. 6 (2015)
14. N.D. Beser, Space data compression standards. Johns Hopkins APL Techn Dig **15**, 206–223 (1994)
15. M. Iliev, C.W. McCluskey, D. Henzlova, et al., Study of the front end electronics contribution to the dead time in He3 proportional counters. Proceedings of the 52nd annual institute of nuclear materials management meeting, California, (2011), p. 17–21
16. Hamamatsu MCP, MCP assembly. http://www.triumf.ca/sites/default/files/Hamamatsu%20MCP%20guide.pdf
17. R.H. Maurer, M.E. Fraeman, M.N. Martin et al., RHarsh environments: space radiation environment, effects, and mitigation. Johns Hopkins APL Tech Dig **28**(1), 17 (2008)
18. P. Adell, G. Allen, *Assessing and mitigating radiation effects in Xilinx FPGAs* (Jet Propulsion Laboratory, California Institute of Technology, Pasadena, 2008)
19. J.J. Wang, Radiation effects in FPGAs. Proceedings of the 9th workshop on electronics for LHC experiments, Amsterdam, Netherlands (2003)